J. Membrane Biol. 214, 19–32 (2006)
DOI: 10.1007/s00232-006-0074-6

The Journal of
Membrane
Biology

The Power of Two-Dimensional Dwell-Time Analysis for Model Discrimination, Temporal Resolution, Multichannel Analysis and Level Detection

Tobias Huth[1], **Indra Schroeder**[2], **Ulf-Peter Hansen**[2]
[1]Department of Physiology, University of Kiel, Olshausenstrasse 40, D-24098 Kiel, Germany
[2]Center of Biochemistry and Molecular Biology, University of Kiel, Leibnizstrasse 11, D-24098 Kiel, Germany

Received: 14 September 2006/Revised: 26 October 2006

Abstract. Two-dimensional (2D) dwell-time analysis of time series of single-channel patch-clamp current was improved by employing a Hinkley detector for jump detection, introducing a genetic fit algorithm, replacing maximum likelihood by a least square criterion, averaging over a field of 9 or 25 bins in the 2D plane and normalizing per measuring time, not per events. Using simulated time series for the generation of the "theoretical" 2D histograms from assumed Markov models enabled the incorporation of the measured filter response and noise. The effects of these improvements were tested with respect to the temporal resolution, accuracy of the determination of the rate constants of the Markov model, sensitivity to noise and requirement of open time and length of the time series. The 2D fit was better than the classical hidden Markov model (HMM) fit in all tested fields. The temporal resolution of the two most efficient algorithms, the 2D fit and the subsequent HMM/beta fit, enabled the determination of rate constants 10 times faster than the corner frequency of the low-pass filter. The 2D fit was much less sensitive to noise. The requirement of computing time is a problem of the 2D fit (100 times that of the HMM fit) but can now be handled by personal computers. The studies revealed a fringe benefit of 2D analysis: it can reveal the "true" single-channel current when the filter has reduced the apparent current level by averaging over undetected fast gating.

Key words: Anti-aliasing filter — Beta distribution — Fast gating — Genetic algorithm — Hidden Markov model — Ion channel — Maximum likelihood — Rate constant

Correspondence to: U.-P. Hansen; email: uphansen@zbm.uni-kiel.de

Introduction

Physiological function of ion channels is determined by channel number, single-channel current and gating. Short-term adaptation of transport rate to physiological needs is mainly achieved by gating, i.e., by spontaneous or agent-induced transitions between conducting and nonconducting states. Malfunctions of these processes lead to severe diseases (Ashcroft, 2000). Even though the knowledge of crystal structure (Doyle et al., 1998; Jiang et al., 2002; Long, Campbell & MacKinnon, 2005a, 2005b) has opened the way to an understanding of structure/function relationships, the interactions between the conformational changes of the channel protein and physiological phenomena like conductivity and gating behavior are still a widely unknown field of channel biophysics. Establishing such a structure/function relationship requires a mathematical description of the gating properties of the channel. This is mainly achieved by means of Markov models (Korn & Horn, 1988; Yeo et al., 1988; Kienker, 1989; Ball & Rice, 1992; Blunck et al., 1998) because it is expected that the states of the Markov model correspond to individual conformational states or groups of equivalent conformational states of the protein. In these approaches, it is assumed that the rate constants of the transitions between the states of the Markov model correspond to the rates of conformational rearrangements in the protein.

Unfortunately, many of the interesting effects are related to rate constants which are at or beyond the limit of the present temporal resolution. Examples are the anomalous mole fraction effect (Farokhi, Keunecke & Hansen, 2000; Hansen et al., 2003), the occurrence of false sublevels which are caused by averaging over fast gating (Schroeder et al., 2004) or the stepwise opening of the selectivity filter (Zheng, Venkataramanan & Sigworth, 2001). Thus, the desire

of high temporal resolution gains increasing importance.

There are three main approaches for the extraction of a Markov model of the channel and its rate constants from the time series of patch-clamp records: dwell-time analysis (Sakmann & Neher, 1995; Blunck et al., 1998), direct fit of the time series (hidden Markov model [HMM]) (Fredkin & Rice, 1992; Albertsen & Hansen, 1994; Klein, Timmer & Honerkamp, 1997; Michalek et al., 1999) and beta distributions (FitzHugh, 1983; Yellen, 1984; Klieber & Gradmann, 1993; Riessner, 1998).

Up to now, the direct fit of the time series, based on a one-step prediction algorithm for the transitions in an HMM (HMM fit), was the most powerful approach, reaching a temporal resolution of about 10 μs (Parzefall et al., 1998; Farokhi et al., 2000; Zheng et al., 2001; Hansen et al., 2003). The most sophisticated version of the HMM fit has been furnished by Venkataramanan, Kuc & Sigworth (1998a, 1998b, 2000), which accounts for the filter response, colored noise, open-channel noise and drift of the base line (Venkataramanan & Sigworth, 2002). This general concept has been modified by other authors, mainly in order to shorten computing time (Michalek et al., 1999; Qin, Auerbach & Sachs, 2000; Fredkin & Rice, 2001).

An alternative line of algorithms is based on the beta fit, i.e., fitting the deviations of amplitude histograms from gaussians by means of beta distributions (FitzHugh, 1983; Yellen, 1984; Klieber & Gradmann, 1993; Riessner, 1998; White & Ridout, 1998; Schroeder & Hansen, 2006). However, this approach is restricted to fast rate constants and often fails if applied to Markov models with more than two states (White & Ridout, 1998; Schroeder et al., 2005). In order to extend the analysis to models with a higher number of states and a mixture of slow and fast rate constants, Schroeder et al. (2005) combined HMM fit and beta fit. They could reach a temporal resolution of about 1 μs.

Here, we deal with the third approach starting from dwell-time analysis, which still is the most widely employed approach (Ball & Sansom, 1989; Sakmann & Neher, 1995; Blunck et al., 1998; Rosales, Fitzgerald & Hladky, 2002). However, the temporal resolution of dwell-time analysis is severely restricted by the temporal resolution of the inevitable jump detector (Schultze & Draber, 1993). Several attempts have been made to improve temporal resolution by so-called missed-events corrections (Yeo et al., 1988; Crouzy & Sigworth, 1990; Hawkes, Jalali & Colquhoun, 1992; Ball et al., 1993; Draber & Schultze, 1994). However, Farokhi et al. (2000) have found a range of independence of the evaluated rate constants on the "true" rate constants (see below). This prevents the applicability of correction algorithms.

Dwell-time analysis can become more powerful if two-dimensional (2D) histograms are evaluated (Magleby & Weiss, 1990a, 1990b). This approach circumvents the mathematical difficulties of incorporating the properties of the jump detector, the anti-aliasing filter and the noise by using simulated time series for the generation of the "theoretical" 2D histogram. Here, we introduce some modifications, i.e., usage of a Hinkley detector (Schultze & Draber, 1993) for jump detection, a genetic algorithm for guiding the fit routine, replacing the maximum likelihood by least square as a convergence criterion and normalizing by the recording time. With these improvements, this approach reaches the temporal resolution of the subsequent HMM/beta (SQ) fit of Schroeder et al. (2005). It seems to be more efficient at model discrimination than the SQ fit. Furthermore, it offers an alternative approach to the determination of the true single-channel current (Schroeder & Hansen, 2006), which becomes important if the true single-channel current is reduced to the apparent current. This reduction occurs if gating becomes faster than the corner frequency of the anti-aliasing filter (Hansen, Keunecke & Blunck, 1997; Townsend & Horn, 1999; Hille, 2001). Another important benefit over the direct fit of the time series (HMM) (Fredkin & Rice, 1992; Albertsen & Hansen, 1994; Klein et al., 1997; Michalek et al., 1999; Venkataramanan & Sigworth, 2002; Schroeder et al., 2005) is the small increase of computing time in multichannel analysis (only about 10% per additional channel).

The algorithms developed here can also be applied to nonstationary time series as obtained from depolarization-induced responses in Na^+ channels, which will be shown in a subsequent report (Huth et al., unpublished data).

Mathematical Tools

The HMM Fit

The HMM fit and its combination with the beta fit (SQ fit) are employed here for the sake of comparison. As it is described in detail by Schroeder et al. (2005), only a short summary is given here. For the HMM fit, the likelihood (L) is calculated as follows:

$$L = \prod_{k=1}^{N_s} \sum_{B=1}^{M} a_k(B) \tag{1}$$

with N_S being the number of samples of the measured time series. Using the concept of merging several identical channels into one macrochannel (Colquhoun & Hawkes, 1977, 1990; Blunck et al., 1998), multichannel records can also be analyzed. $M = m^N$ is the number of states of the macrochannel, representing N

channels with m states. The probability of $a_k(B)$ being in state B at time $t = jT$ ($j = k, k-1$) is calculated recursively as follows:

$$a_k(B) = \sum_{A=1}^{M} a_{k-1}(B) p_{AB} f_B(I_k) \quad (2)$$

with p_{AB} being the probability of a transition from state A to state B. $f_B(I_k)$ is the probability that the current I_k measured at time $t_k = kT$ can be assigned to state B. This is done by splitting the overall amplitude histogram into gaussian distributions per level (Schroeder et al., 2004). A fitting routine, here a simplex algorithm (Caceci & Cacheris, 1984), varies the rate constants k_{AB} of the assumed Markov model, which determine p_{AB} (*see* Albertsen & Hansen, 1994) until a maximum L is found. Thus, the outcome of the procedure is a set of k_{AB}.

Multistate, Multichannel Beta Distributions for Higher-Order Filters

Amplitude histograms can deviate from gaussian distributions when gating beyond the filter frequency occurs in the time series. They can be evaluated by means of beta distributions (FitzHugh, 1983). Utilizing the increase of computer power, it became possible to use simulations for the "theoretical" amplitude histograms of patch-clamp currents attenuated by higher-order filters, enabling analysis of multistate, multichannel Markov models. Thus, time series were generated by simulations as described below, and the amplitude histograms were generated by standard procedures.

In the SQ fit, first a HMM fit was done, and the results were used as starting values for a beta fit. The slow rate constants were kept constant and only the fast rate constants (above one-fourth of the filter frequency) were varied under the guidance of a simplex algorithm to find the best fit. Details are given by Schroeder et al. (2005).

1D Fit

One-dimensional dwell-time histograms were created by standard procedures (Sakmann & Neher, 1995) and fitted by a sum of exponentials (Blunck et al., 1998):

$$f(t) = \sum a_i \exp\left(\frac{t}{\tau_i}\right) \quad (3)$$

with a_i being the amplitude factor and τ_i being the time constant by means of the program Kiel-Patch (available at http://www.zbm.uni-kiel.de/software).

Creating 2D Dwell-Time Histograms

Dwell-time histograms were generated as described by Magleby & Weiss (1990b). Pairs of dwell times obtained from an open event with dwell time of τ_O and a subsequent closed event with dwell-time τ_C were assigned to a 2D bin in the τ_O/τ_C plane using the log-binning technique (McManus, Blatz & Magleby, 1987) with 10 bins per decade. If microreversibility is assumed, the open/closed histograms coincide with closed/open histograms.

Fit Algorithms

A fitting routine has to be guided by an algorithm which suggests a sequence of parameter sets in such a way that the path through the parameter space leads to the global optimum (the best parameter set). In previous reports (Farokhi et al., 2000; Hansen et al., 2003; Schroeder et al., 2005), the simplex algorithm (Caceci & Cacheris, 1984; Press et al., 1989) was found to be quite efficient. A simplex moves like an ameba through the parameter space. Nevertheless, the genetic algorithm (Rechenberg, 1973; Holland, 1975) turned out to have a higher chance of finding the global optimum. It works on a population of parameter sets and seeks to find the best set by methods which are similar to those of biological evolution, namely spontaneous mutation, sex (crossover) and selection of the fittest. This strategy seems to have a better chance of finding the global optimum than the simplex algorithm (Charbonneau, 2002). The software for this work used the GAlib genetic algorithm package, written by Matthew Wall at the Massachusetts Institute of Technology (Wall, 1996) with the specifications and settings shown in Tables 1 and 2.

The parameters (rate constant k_{AB}) are coded by 16-bit numbers. A mutation converts a "1" to a "0" or vice versa. Crossover breaks two adjacent genes (parameter sets) at the same length and builds two new genes from the four parts by cross-wise combination. Selection determines which of the parent generation and which of the children are allowed to survive.

Choice of the Convergence Criterion

There are two mean convergence criteria employed in fitting routines. Maximum likelihood (ML) was used by Magleby & Weiss (1990a):

$$\log L = \sum_{i,j}^{N} \log\left(\frac{M_{ij} H_{ij}}{N}\right) \text{ for } M_{ij} > 0 \quad (4)$$

with H_{ij} being the occupation of bin (i,j) in the theoretical 2D dwell-time histogram (hypothesis, obtained from the assumed Markov model by

Table 1. Specification of the genetic fit algorithm

Type of genetic algorithm	GASimpleGA (nonoverlapping populations)
Definition of the genome	GARealGenome (real numbers)
Initialization	UniformInitializer (equally distributed coverage of the parameter space)
Mutation	GARealGaussianMutator (The probability of parameter changes is under the control of a gaussian distribution, making small changes more likely.)
Crossover	UniformCrossover (Each gene is selected randomly from the parent genes.)
Selection	GARouletteWheelSelector (This selection method picks an individual based on the magnitude of the fitness score relative to the rest of the population. The higher the score, the more likely an individual will be selected. Any individual has a probability p of being chosen, where p is equal to the fitness of the individual divided by the sum of the fitnesses of each individual in the population.)

The software for this work used the GAlib genetic algorithm package, written by Matthew Wall (1996) at the Massachusetts Institute of Technology. The specifications as depicted in the table are used for the 2D fit algorithm. The descriptions of the specifications used here are taken from the manual of GAlib.

Table 2. Standard settings for the genetic algorithm

Number of population members with uniform distribution over the parameter space	250
Maximum generation number	10,000
Mutation rate, parameter mutations are gaussian distributed	0.010
Crossover rate	0.60
Coding of parameters, real parameters	16 Bit
Stop criterion (number of generations without improvement of the fitness)	50
Selection (Any individual has a probability p of being chosen, where p is equal to the fitness of the individual divided by the sum of the fitnesses of each individual in the population.)	Roulette-Wheel
Ratio n (length of simulated time series/measured time series)	$n = 1$

The software for this work used the GAlib genetic algorithm package, written by Matthew Wall (1996) at the Massachusetts Institute of Technology. All but the last line are standard parameters of the genetic algorithm that can be adjusted for fitting purposes. We found the parameters to work well for our application. For larger Markov models with more free parameters, one should consider an increase of the population size, which increases fitting time disproportionally. For short measured time series, one can increase the ratio (last line), which reduces the statistical impact of the simulated time series.

simulations), M_{ij} being occupation of bin (i,j) in the measured 2D dwell-time histogram, N being the number of simulated events (as done by Magleby & Weiss, 1990a).

Here, we mainly use the least square (LS) criterion:

$$E^2 = \sum_{i,j}^{N} (M_{ij} - H_{ij} \frac{T_{mes}}{T_{sim}})^2 \tag{5}$$

with E being the error, M and H as defined above, T_{mes} and T_{sim} being the durations of the measured and the simulated time series, respectively.

In some investigations, averaging over 9 or 25 bins is done (9- or 25-bin method):

$$E^2 = \sum_{i,j} \left(\sum_{u=i-m}^{i+m} \sum_{v=j-m}^{j+m} M_{uv} - \sum_{u=i-m}^{i+m} \sum_{v=j-m}^{j+m} \frac{T_{mes}}{T_{sim}} H_{uv} \right)^2 \tag{6}$$

with $m = 1$ for 9 bins and $m = 2$ for 25 bins.

Simulations of Time Series

The basic algorithm for the generation of simulated time series (surrogate data) has been described previously (Riessner et al., 2002; Schroeder et al., 2005). Briefly, it starts from an assumed state in the selected Markov model: the dwell time in this state and the aim of the next jump are estimated from the assumed rate constants under the guidance of two random number generators. The system remains in this state for the estimated dwell time. After the jump has occurred, the calculations of the dwell time and the aim of the jump are repeated. Continuous application of this procedure results in the surrogate time series of the selected Markov model. The resulting signal is subject to the same filtering process as applied to the measured data. The filtered Markov signal is superimposed by noise. The noise is obtained from a jump-free time series of the patch-clamp record which is to be analyzed, in contrast to previous reports where artificially produced noise was used. In all investigations, the length of the simulated time series is equal to that of the measured one.

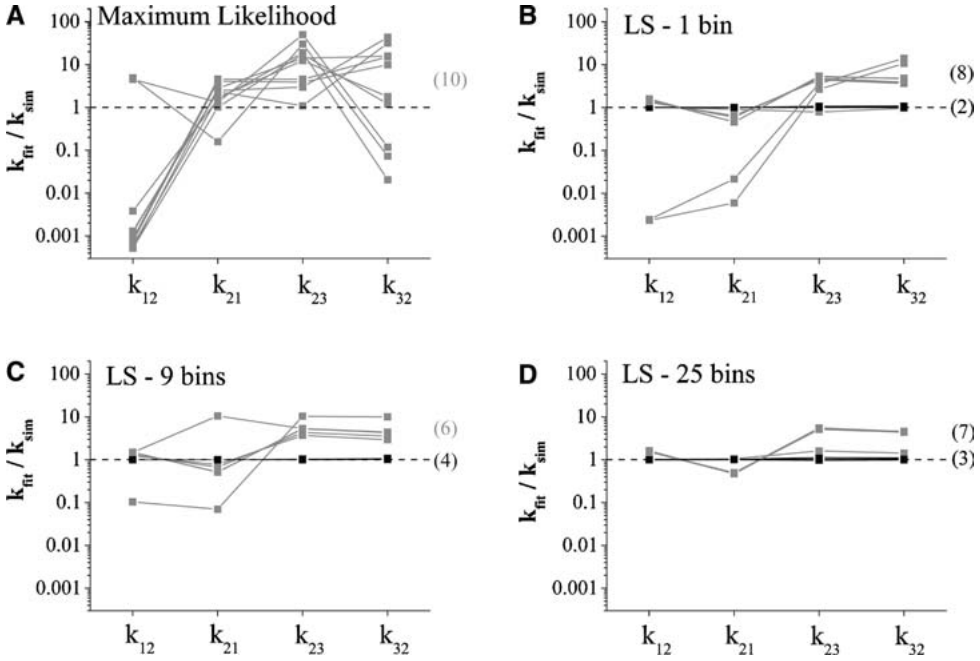

Fig. 1. Dependence of fit results on the error criterion. Rate constants of "measured data" (equation 7) and simulated data obtained from fitting results were compared. Different convergence criteria were used by the fitting routine: (*A*) the maximum likelihood (equation 4) or (*B-D*) the least square (LS, equation 5) criterion. In some LS fits, the average of neighboring bins was used, with (*C*) 9 bins or (*D*) 25 bins (LS, equation 6) in order to reduce the statistical variability. The "measured" time series was obtained from a simulation by means of the model in equation 7. Each graph shows the results of 10 fits. The rate constants related to one fit result are connected by lines. Fits were guided by a simplex algorithm. The numbers in parentheses give the number of parameter sets presented by the adjacent group of curves. *Black traces* indicate good fits close to the ratio of 1 for k_{fit}/k_{sim}. *Gray traces* indicate fits with k_{fit} deviating significantly from k_{sim}.

Results

Efficiency of the Convergence Criterion

The efficiency of different convergence criteria for 2D dwell-time analysis (equation 4 *vs*. equations 5 and 6) was compared by means of time series which were simulated from the following three-state model:

$$C_1 \underset{2000s^{-1}}{\overset{2000s^{-1}}{\rightleftharpoons}} O_2 \underset{200s^{-1}}{\overset{200s^{-1}}{\rightleftharpoons}} C_3 \qquad (7)$$

The first approach maximized the maximum likelihood as a convergence criterion (equation 4). The other ones minimized the sum of least squares and differed with respect to averaging. In the τ_C,τ_O plane, averages of the number of observed transitions were taken from rectangular fields of 1, 9 or 25 bins (equations 5 and 6).

Figure 1 shows the effect of the convergence criterion on the accuracy of determining the rate constants. Ten time series were generated from simulations on the basis of the three-state model in equation 7. 2D dwell-time analysis was done of each single time series as described above using the four different convergence criteria (equations 4–6). The variability of the repetitive fits resulted from the fact that the "theoretical" time series had to be generated by simulations which depend on a random generator. This illustrated the necessity to repeat the fits several times in order to discard incorrect fitting results, which were indicated by higher error sums. The success of the fits was described by the ratio of the rate constant k_{fit} obtained from the fit and the rate constant k_{sim} used in the simulation of the "measured" time series. The ML approach (equation 4) did not result in any correct solution (Fig. 1A). The LS criterion without averaging (1 bin) resulted in two perfect fits, six of which were at least better than those of ML and two of which failed (Fig. 1B). LS with averaging over 9 bins provided already four perfect fits and six that were better than those of the previous approaches (Fig. 1C). The errors become even smaller with averaging over 25 bins (Fig. 1D). Fig. 1A shows that ML may not always be the first choice in fitting problems. In 2D dwell-time analysis, it encounters special problems if bins in the τ_C,τ_O plane are empty. They have to be excluded because multiplication by 0 or the logarithm of 0 would invalidate the calculation of the ML. Nevertheless, in the next paragraph it is shown that ML does slightly better with respect to the separation of closefitting results.

The width of the field in the τ_C,τ_O plane used for averaging depends on the temporal resolution

necessary for analysis of the measured data. Thus, it is recommended that some investigations be done with simulated data in order to find the optimal width of the field. The simulations should make use of a set of the rate constants obtained from a first fit. Then, a new set should be created with faster rate constants in order to test whether faster rate constants in the measured time series would have been detected.

Accuracy of Determining Rate Constants

An important feature of any fit program is the magnitude of $\partial C/\partial k_{ij}$, i.e., the dependence of the convergence criterion C on the parameters k_{ij} that have to be determined. In order to evaluate the effect of the choice of the convergence criterion on the accuracy of parameter determination, simulations were done using the following five-state model.

$$C_1 \underset{k_{21}}{\overset{2500s^{-1}}{\rightleftharpoons}} O_2 \underset{5000s^{-1}}{\overset{5000s^{-1}}{\rightleftharpoons}} O_3 \underset{1000s^{-1}}{\overset{1000s^{-1}}{\rightleftharpoons}} C_4 \underset{50s^{-1}}{\overset{2000s^{-1}}{\rightleftharpoons}} C_5 \qquad (8)$$

A so-called measured time series was simulated with $k_{21} = 50 \cdot s^{-1}$, $T_{sim} = T_{mes} = 25$ s at 200 kHz sampling rate and an anti-aliasing filter of 50 kHz. This time series was compared with "theoretical" time series with equal rate constants besides k_{21}. The variable rate constant k_{21} was set to seven different values ranging from $50 \cdot s^{-1}$ (the value of the "measured" time series) to $1{,}050 \cdot s^{-1}$. For each value of k_{21}, 5,000 simulated time series were generated. From these time series, 2D histograms were generated. The "measured" and "theoretical" histograms were compared using the four different convergence criteria also employed in Figure 1.

In Figure 2, error histograms are shown; i.e., the numbers of simulations yielding the error sum given at the abscissa were plotted on the y axis. Logarithmic binning was employed. The slight increases in the height of the peaks in Figure 2B–D indicate that the distribution of errors becomes narrower in terms of the relative deviation from the mean error sum. The degree of overlap of the error histograms in Figure 2 gives an estimate of the chance to distinguish different parameter values by the employed fitting routine.

Figure 2 shows that $k_{21} = 50 \cdot s^{-1}$ and $k_{21} = 60 \cdot s^{-1}$ cannot be distinguished under all four convergence criteria because the density functions overlap completely. The ML estimator (Fig. 2A) gives the best separation for $k_{21} = 100 \cdot s^{-1}$, while for $k_{21} = 150 \cdot s^{-1}$ the 25-bin LS criterion (Fig. 2D) does better. This superiority of the LS criterion holds especially for all higher values of k_{21}. The conclusion from Figure 2 is that ML could discriminate close values of k_{21} better than LS, whereas the LS criteria are more efficient at greater differences. Averaging over bins (9 and 25) leads to better discrimination for close k_{21}. The difference between 9- and 25-bin averaging is small. If the density distributions overlap partially, the fits have to be repeated several times in order to reveal the shape of the "error histograms" and thus to achieve a separation of the solutions. Figure 2E provides another presentation of the results: the dependence of the error sums on the deviation of the rate constant from its correct value is steepest for the 25-bin LS approach.

Figure 2A also provides a suggestion of why the ML criterion may fail. There is overlap of the distributions even at strong deviations, which does not occur with the LS criterion. Because of this, the fit routine may already be misled far away from the correct values. However, in close neighborhood of the correct values, the ML approach may do better.

The results may be surprising as ML seems to be the more trendy approach among modern mathematicians. Nevertheless, there are many examples which show that the superiority of ML is not always given (Singh & Sutradhar, 1989; Ganesan & Sherman, 1994). Besides the possibility of preaveraging (equation 6), there may be another reason for the better performance of the LS criterion: in correlation analysis, cross-correlation functions and cross-structure functions are used. Equation 4 corresponds to a 2D cross-correlation function because

$$CCF_{(0,0)} = \sum_{i,j} M_{ij} H_{ij} \qquad (9)$$

In contrast, equation 5 is a cross-structure function. Comparison of equations 4 and 5 shows that the cross-correlation function is generated from the mixed term in equation 5. Schulz-DuBois & Rehberg (1981) have shown that structure functions (equation 5) are by far less sensitive to drift and more sensitive to detecting characteristic features than correlation functions are.

Temporal Resolution

Patch-clamp amplifiers comprise a low-pass filter whose cut-off frequency may be determined by different constraints, e.g., frequency response of the amplifier, anti-aliasing, noise reduction or preferences of the investigator. This filter limits the temporal resolution when Markov models with fast gating processes are to be investigated. Different methods provide different strengths with respect to temporal resolution: Farokhi et al. (2000) found that the HMM fit provided sufficient temporal resolution in order to reveal fast gating as the origin of current reduction in the anomalous mole fraction effect of the K^+ channel in *Chara*, whereas 1D dwell-time distributions failed. Schroeder et al. (2004) constructed amplitude distributions per level and detected rate

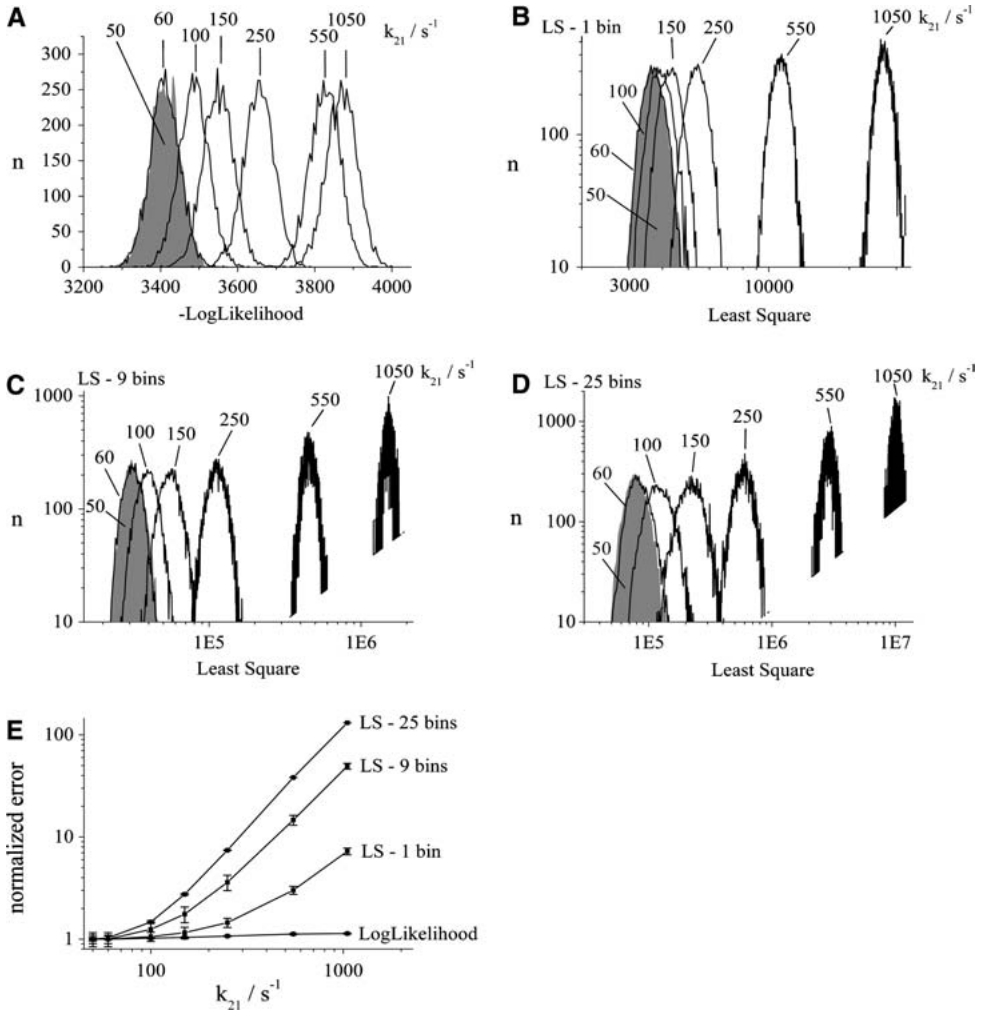

Fig. 2. "Error histograms" showing the distribution of errors depending on the criterion. A "measured" time series according to the model of equation 8 was simulated with $k_{21} = 50 \cdot s^{-1}$. For the "theoretical" time series, different values of k_{21} were assumed as indicated at the curves. For each value of k_{21}, 5,000 time series were simulated, and the difference between the 2D histogram of the "measured" and the "theoretical" time series was calculated by means of equation 4 (*A*) or equations 5 and 6 (*B–D*). Error sums were grouped in bins. The bin width was proportional to the error sum, with the bin width at the maximum of the distribution for $k_{21} = 50 \cdot s^{-1}$ having the following values: *A*, 5; *B*, 50; *C*, 50; *D*, 200. The number of fits resulting in an error sum falling into such a bin is plotted on the *y* axis. The missing data points in *C* and *D* are caused by rounding effects. The trace with the gray area under the curve is the distribution for the k_{21} which was identical to that of the "measured"time series ($50 \cdot s^{-1}$). (*E*) Dependence of the error criterion on the deviation of the assumed rate constant from the "true" one.

constants on the order of $10^6 \cdot s^{-1}$ in *Chara* recorded with a sampling rate of 200 kHz and a four-pole Bessel filter of 50 kHz. The same result was obtained with a subsequent HMM and amplitude fit using beta distributions (Schroeder et al., 2005).

As discussed above (*see* Introduction), there are different approaches to extend the range of accessible gating processes. Here, it is shown that also 2D dwell-time analysis has the power to look beyond the filter frequency (as already shown by Magleby & Weiss, 1990a). In order to demonstrate the performance with respect to the detection of fast gating, we use a simple two-state model where interference from the other states is excluded. As fast gating often is restricted to one transition, the usage of the following two-state model accounts for the majority of scenarios:

$$C_1 \underset{k_{21}}{\overset{k_{12}}{\rightleftharpoons}} O_2 \tag{10}$$

Time series were simulated with $k_{12} = k_{21}$ in the range 2,500–500,000 $\cdot s^{-1}$ with five replicates per pair of rate constants, and the time series were analyzed by 1D dwell-time fit, HMM fit, subsequent HMM and beta fit and 2D dwell-time analysis. The ratio between simulated (true) value of $k_{12} = k_{21} = k_{sim}$ and k_{fit} obtained from the fitting routines is plotted *vs.* k_{sim} in Figure 3A.

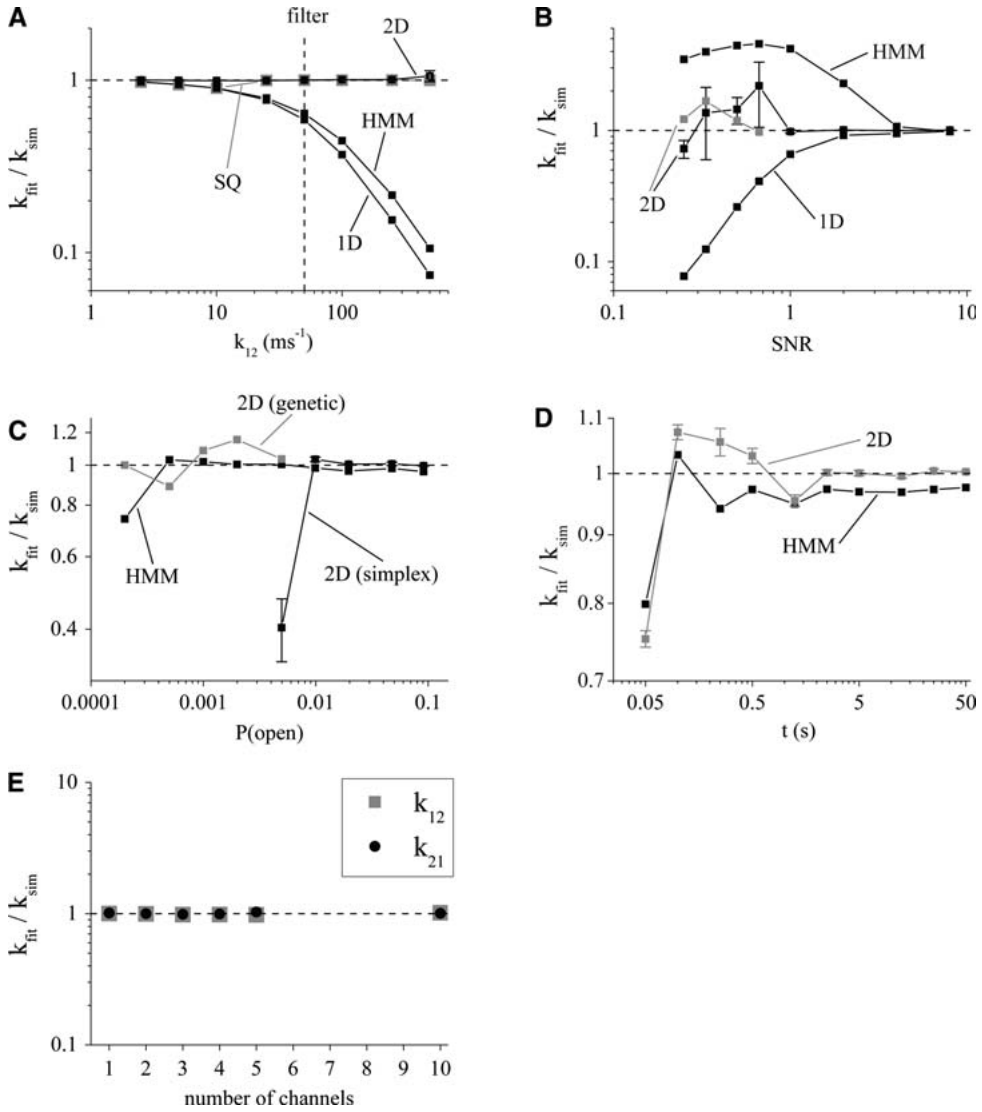

Fig. 3. Performance of different fit strategies dependent on characteristic parameters of patch-clamp data. For all tests, a simple C-O Markov model (equation 10) was used to simulate the ''measured'' time series. It was analyzed by the 2D fit algorithm (2D), a 1D dwell-time fit (1D), a HMM fit (HMM) and an SQ fit (SQ). There are no error bars at the results of the HMM and 1D fit because these are analytical approaches, where repetitive fits yield identical results. *Dashed horizontal lines* indicate correct solutions ($k_{fit}/k_{sim} = 1$). Unless otherwise stated, the settings were as follows: filter frequency = 50 kHz, sampling = 200 kHz, $k_{12} = k_{21} = 2{,}500 \cdot s^{-1}$, length of the time series $t_s = 50$ s, SNR = 8; error calculation for the 2D fit was done with the LS method (9 bins). Because of the simple model, a faster simplex algorithm was employed unless otherwise stated. (*A*) Dependence on rate constants $k_{12} = k_{21}$ as given on the abscissa. The filter frequency is presented by a *vertical dashed line*. (*B*) Dependence on noise presented as SNR at the abscissa. Below SNR = 1, the genetic algorithm was applied for the 2D fit (2D genetic grey), leading to better results compared to the simplex algorithm (2D simplex black). (*C*) Dependence on the occupation probability of the open state, $P_{open} = k_{12}/(k_{12} + k_{21})$. The open probability was decreased by lowering k_{12}. k_{21} was set to $5{,}000 \cdot s^{-1}$. (*D*) Influence of the length of the time series on the genetic 2D fit and the HMM. (*E*) Dependence on channel number. Time series of *n* channels (abscissa) were generated by simulation and subjected to a 2D dwell-time fit as defined in the Mathematical Tools section.

Figure 3A shows that the 1D fit and the HMM fit do not find the correct values when the rate constants exceed the cut-off frequency of the filter (given by the vertical line). The descending trace k_{fit}/k_{sim} approaches the slope −1. This means k_{fit} is constant and independent of the original value of k_{sim} (compare Farokhi et al., 2000). The small difference between the 1D fit and the HMM fit was surprising. The HMM fit did much better in the investigations of Farokhi et al. (2000), probably because they checked the results by simulations. In contrast, the 2D fit and the SQ fit find the correct rate constants up to $500 \cdot ms^{-1}$ (where the investigation ended because of computing time requirements). In the case of the SQ fit, there is a dip of k_{fit}/k_{sim} at medium rate constants. In this range, the accuracy of the HMM fit starts to

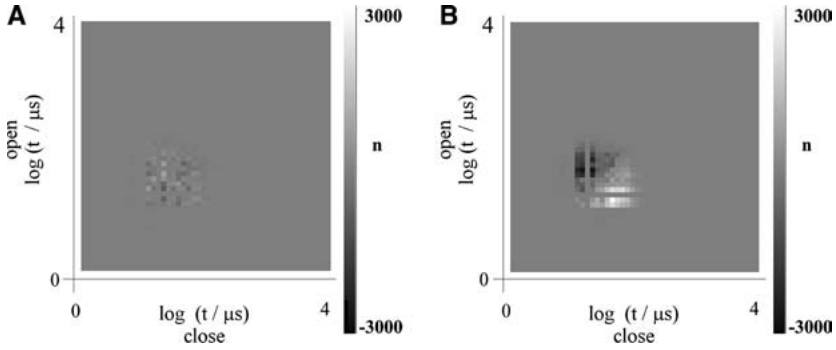

Fig. 4. 2D difference histograms showing the sensitivity of the 2D fit to rate constants beyond the filter frequency. Two time series were simulated for each diagram with a simple C-O Markov model with the following settings: filter frequency = 50 kHz, sampling rate = 200 kHz, length of the time series t_s = 250 s, SNR = 8. 2D dwell-time histograms were constructed, and the difference histogram was calculated. Difference histograms were generated from two time series (*A*) both generated from the same two-state model of equation 11 with $k_{12} = k_{21} = 200 \cdot \text{ms}^{-1}$ or (*B*) generated from two different two-state models with the same $k_{21} = 200 \cdot \text{ms}^{-1}$ but different k_{12}, being $200 \cdot \text{ms}^{-1}$ and $205 \cdot \text{ms}^{-1}$, respectively. The gray background stands for zero deviation. Areas which are whiter indicate that the error difference is positive and those that are darker, that it is negative.

suffer from the filter and the deviations of the amplitude histogram from that of the baseline noise are not yet strong enough. This leads to a misestimation of 10% at $k_{12} = 10 \cdot \text{ms}^{-1}$.

Determining rate constants beyond the filter frequency may be surprising. Figure 4 shows that differences between theoretical and ''measured'' rate constants far beyond the filter frequency (50 kHz) lead to significant differences in the 2D plots. The ''measured'' time series was generated from model I

$$C_1 \underset{200ms^{-1}}{\overset{200ms^{-1}}{\rightleftharpoons}} O_2 \tag{11}$$

by simulation. First, the measured time series was compared with the theoretical time series simulated from the same model. The small differences in Figure 4A resulted from statistical variations due to the finite length of the time series ($5 * 10^7$ data points). In a second run, the ''measured'' time series was compared with a time series where $k_{12} = 200 \cdot \text{ms}^{-1}$ was replaced by $k_{12} = 205 \cdot \text{ms}^{-1}$. Figure 4B shows that significant differences occurred in the difference histogram. This is the basis for the fit routines to determine also rate constants beyond the filter frequency.

The question may come up of what the theoretical background is that an algorithm can find rate constants with nominal values beyond the filter frequency. It has to be recognized that the dwell time of sojourns in a state are exponentially distributed. Because of this, there are always events in the tail of the distribution which can be detected by the Hinkley detector. Furthermore, bursts of undetected fast flickering cause apparent open and closed dwell times in the measured time series which should be reproduced by the theoretical time series.

Sensitivity to Noise

''Measured'' time series were obtained from simulation of a C-O model (equation 10) with the rate constants $k_{12} = k_{21} = 2{,}500 \cdot \text{s}^{-1}$ and superimposed by noise of a different signal-to-noise ratio (SNR) as given on the abscissa of Figure 3B. Artificial white noise was produced as described by Riessner et al. (2002). 1D, 2D and HMM fits were performed as described above. The 2D fit used the LS sum as a convergence criterion with preaveraging over a field of 9 bins. The fitting procedure was guided by a simplex algorithm (black trace in Fig. 3B) or by a genetic algorithm (gray trace in Fig. 3B). Figure 3B shows that the 2D fit (especially that one using the genetic algorithm) is much less sensitive to noise and still yields reasonable results at an SNR of 0.5.

Minimum Probability of Sojourns in a Given State

Low occupation probability in one state is an important scenario for certain types of ion channel, like voltage-activated sodium channels. In the following two-state model,

$$C_1 \underset{5000s^{-1}}{\overset{k_{12}}{\rightleftharpoons}} O_2 \tag{12}$$

k_{12} was changed between 1 and $500 \cdot \text{s}^{-1}$ in order to change the probability of the occupation of the open state as given on the abscissa of Figure 3C ($P_{\text{open}} = k_{12}/[k_{12} + k_{21}]$). It was found that the genetic 2D fit gave reasonable results even at an occupation probability of $2 * 10^{-4}$ (Fig. 3C). The HMM fit seemed to need longer occupation times of the open state. However, if the occupation time was long enough, the accuracy was better. The 2D fit guided by

a simplex routine required much longer occupation times.

Length of the Time Series

The performances of the HMM fit and of the 2D fit (9 bins) were about equal with respect to the length of the time series (Fig. 3D). However, the accuracy of the 2D fit was higher, probably caused by the feature that the "theoretical" data of the 2D fit were generated by simulations.

Multichannel Analysis

Time series with up to 10 channels of a two-state model with $k_{12} = 100 \cdot s^{-1}$ and $k_{21} = 5{,}000 \cdot s^{-1}$ were generated as stated in the legend of Figure 3E. 2D dwell-time histograms were generated from the events detected by a multilevel Hinkley detector (Schultze & Draber, 1993). Events at all current levels were merged into a single 2D histogram; i.e., it was composed of all jumps from level n to level $n + 1$ and *vice versa*. This may appear to be an unconventional approach. However, since it was done for the "theoretical" and for the "measured" time series in the same way, it could be used for the calculation of the error sum (equations 5 and 6). The direction of the sequence of two adjacent dwell times in level n and $n + 1$ can be ignored in stationary time series where microreversibility allows the inversion of the time scale.

Figure 3E shows that the analysis yields reliable results in all simulations from one to 10 channels. The computing time increased by about 10% per additional channel. This small increase results from the following features: generation of more events in the time series is only a minor part of the whole simulation procedure. This also holds for jump detection by the Hinkley detector as these processes occur in the cache of the processor. Furthermore, the time consumption of superposition with noise and filtering is independent of channel number.

Model Discrimination

One stronghold of the analysis of 2D dwell-time histograms is its ability to distinguish Markov models which cannot be distinguished by 1D analysis (Magleby & Weiss, 1990b). The feature results from the fact that the occurrence of a short closed event may have a higher probability when the preceding state was O_1 and not O_2 depending on the actual Markov model. The HMM fit, too, considers the probabilities of transitions from individual source states to individual sink states; thus, the same ability to distinguish models should be expected (Fredkin & Rice, 1992; Caliebe, Rösler & Hansen, 2002; Loeptin, 1999).

However, we show that the 2D fit based on simulations yields a better model discrimination than the classical HMM fit. The "measured" data were obtained from a situation that applies to channels which are activated by a stimulus, e.g. by a depolarization as in the case of Na^+ channels. The Markov model of the "measured" time series is as follows:

$$C_1 \underset{50s^{-1}}{\overset{2500s^{-1}}{\rightleftharpoons}} O_2 \underset{5000s^{-1}}{\overset{5000s^{-1}}{\rightleftharpoons}} O_3 \underset{1000s^{-1}}{\overset{1000s^{-1}}{\rightleftharpoons}} C_4 \underset{50s^{-1}}{\overset{2000s^{-1}}{\rightleftharpoons}} C_5 \qquad (13)$$

The time series starts always in C_1 for each simulation and typically ends in C_5. After about 25 ms, open events are hardly observed because of the low transition probability from C_5 to C_4. In order to get enough data, the time series was started 5,000 times in C_1. Because of the control of the transitions by a random generator, all time series were different. For the analysis of such time series, the HMM fit was modified to repetitively start from state C_1.

The analysis made use of three different models. The "true" one with the arrangement of states as in equation 13 and two nonequivalent models as given by equations 15 and 16:

$$C_1 \underset{k_{21}}{\overset{k_{12}}{\rightleftharpoons}} O_2 \underset{k_{32}}{\overset{k_{23}}{\rightleftharpoons}} O_3 \underset{k_{43}}{\overset{k_{34}}{\rightleftharpoons}} C_4 \underset{k_{54}}{\overset{k_{45}}{\rightleftharpoons}} C_5 \qquad (14)$$

$$C_1 \underset{k_{21}}{\overset{k_{12}}{\rightleftharpoons}} O_2 \underset{k_{32}}{\overset{k_{23}}{\rightleftharpoons}} C_3 \underset{k_{43}}{\overset{k_{34}}{\rightleftharpoons}} O_4 \underset{k_{54}}{\overset{k_{45}}{\rightleftharpoons}} C_5 \qquad (15)$$

$$\begin{array}{l} C_1 \underset{k_{21}}{\overset{k_{12}}{\rightleftharpoons}} O_2 \underset{k_{42}}{\overset{k_{24}}{\rightleftharpoons}} C_4 \underset{k_{54}}{\overset{k_{45}}{\rightleftharpoons}} C_5 \\ \qquad\quad k_{23} \Updownarrow k_{32} \\ \qquad\quad O_3 \end{array} \qquad (16)$$

The starting values k_{ij} were set to $500 \cdot s^{-1}$ for all models in all fits. Figure 5A shows that the HMM fit with the model of equation 15 persistently gave worse fits than the other two models and could be ruled out. However, the "wrong" model of equation 16 could not be rejected by means of the results of Figure 5A.

This rejection was achieved when 2D dwell-time analysis was employed in a two-step fitting routine, starting with a genetic algorithm and finishing with a subsequent simplex algorithm (Fig. 5B). The simplex was used to reach the highest possible fit accuracy. Figure 5B shows that now the "wrong" models of equations 15 and 16 resulted in higher error sums. The minimum possible error, calculated by using simulated time series with the right parameters, is given on the left-hand side of Figure 5B, indicated by an asterisk. Because of the scatter in Figure 5B, it is important to repeat the fits in order to eliminate stochastic variations when separating the models.

Determination of the True Current Level

The determination of the true single-channel current is difficult in noisy data and in the presence of fast

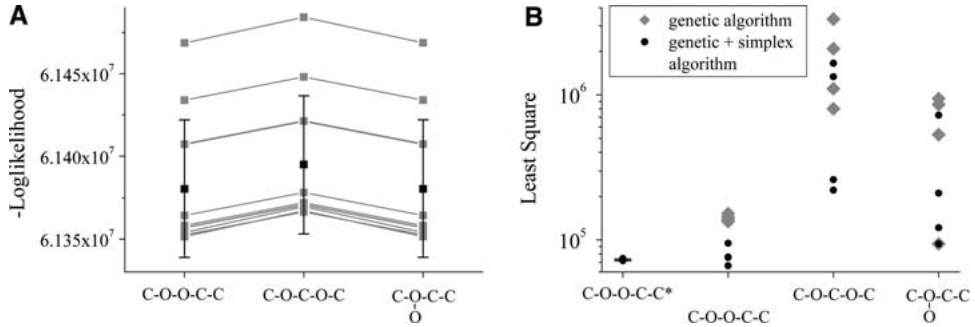

Fig. 5. Model discrimination by the 2D fit and the HMM fit. A time series was simulated with the model of equation 13 as a ''measured'' reference and analyzed with three different Markov models as given on the abscissa (equations 14–16). Each model contained three closed and two open states with a different sequence of states. This test was designed for evoked currents of sodium channels. According to the brief length of these records, only short traces were repeatedly simulated, every time starting at C_1. Filter frequency = 50 kHz, sampling rate = 200 kHz, length of each series = 5,000 depolarization-induced responses of t_s = 25 ms, SNR = 8. Error calculation for the 2D fit was done with the LS method (9 bins). (*A*) HMM fit of 10 time series (*gray traces*) resulting in the log likelihood given at the *y* axis. Results belonging to the same time series are connected. Mean and standard deviation are displayed in black. (*B*) 2D fit of four time series resulting in the LS error given at the *y* axis. In the first step, the genetic algorithm was applied (*gray diamonds*). Then, fitting results were fed as starting values into a simplex algorithm (*black circles*). The error of C-O-O-C-C* is not obtained from fitting but from simulations based on the reference model and yields an estimation of the smallest possible error and the related standard deviation as caused by the random behavior of simulations. For the sake of clarity, points are not connected as in *A*.

gating. Mostly, the peaks of the amplitude histograms are evaluated by fitting the amplitude histograms by a sum of gaussians. However, Riessner et al. (2002) have shown that in noisy data image analysis by the human protein computer is superior to the fitting analysis by silicon computers. Positioning a line in the original time series on the computer screen (e.g., by the program Kiel-Patch) still gave reasonable results where the analysis by means of amplitude histograms failed. However, also this approach fails if fast gating and averaging in the anti-aliasing filter lead to apparent current reduction. Here, a new tool is introduced, making use of 2D dwell-time histograms. This tool enables the detection of the true single-channel current level.

The approach depends on the feature that the true value of the single-channel current has to be told to the Hinkley detector before jump detection can start and that a wrong value may cause improper detection. This is utilized in the following procedure. First an amplitude histogram is generated from the ''measured'' (simulated) time series. Then, 2D dwell-time analysis is employed including the following steps: jump detection with a putative value of the true single-channel current, generation of 2D dwell-time plots, 2D dwell-time analysis delivering a set of rate constants k_{ij}. From these rate constants, a new time series is simulated with the putative single-channel current and the noise as obtained from the measured time series. The amplitude histogram generated from this simulated time series is compared with that of the ''measured'' data. This procedure is repeated for different values of the putative single-channel current.

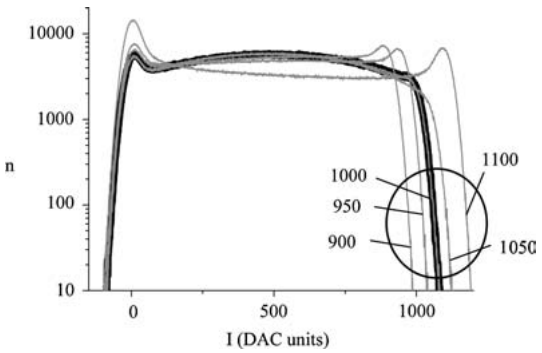

Fig. 6. Detection of the true single-channel current in time series where apparent single-channel current is reduced by fast gating. A ''measured'' time series was generated from a three-state COC Markov model (equation 17) by simulation, and the amplitude histogram of current was constructed (*black trace*). Filter frequency = 50 kHz, sampling rate = 200 kHz, length of the time series = 50 s, SNR = 8 and simulation current level was set to 1,000 DAC units. The ''measured'' time series was analyzed with the 2D fit (LS, 9 bins, genetic algorithm) for different assumed current levels. Using the resulting rate constants, ''theoretical'' time series were simulated and amplitude histograms constructed for each one of these levels (numbers at the *gray traces*).

Figure 6 illustrates the sensitivity of this approach by means of a three-state model as given by the following reaction scheme:

$$C_1 \underset{5ms^{-1}}{\overset{50ms^{-1}}{\rightleftharpoons}} O_2 \underset{200ms^{-1}}{\overset{200ms^{-1}}{\rightleftharpoons}} C_3 \qquad (17)$$

A three-state model was found to be sufficient for the demonstration of performance for the following reasons. A more complex model would consist of

states with long and short dwell times. If long dwell times do occur, the current level related to these states can be determined with high accuracy. Thus, the interesting part of a more complex Markov model is that part where fast gating occurs, and this normally is restricted to a few states (e.g., Farokhi et al., 2000).

For the analysis in Figure 6, a time series simulated from equation 17 with a single-channel current of 1,000 digital to analogue converter (DAC) units is used as the "measured" time series. Its amplitude histogram is presented by the black trace in Figure 6. It is obvious that noise and fast gating prevented the determination of single-channel currents on the right-hand side of the diagram, whereas it was possible on the left-hand side, which is attributed to the slower rate constants of the first closed state.

The gray lines are assigned to amplitude histograms obtained from the results of the 2D fit with different putative single-channel currents. Figure 6 shows that only the amplitude histogram (1,000 DAC units) generated with the correct single-channel current (and with the correct rate constants of the Markov model obtained by the 2D fit algorithm) coincides with the amplitude histogram of the measured time series. Already a deviation of 5% in single-channel current results in significant deviations from the amplitude histogram of the measured time series.

Conclusions

The 2D dwell-time analysis presented above turned out to belong to the group of the most powerful tools for the analysis of patch-clamp time series. Its efficiency is much higher than that of the pure classical HMM fit (Albertsen & Hansen, 1994) or the conventional 1D dwell-time fit (Blunck et al., 1998). Comparison with the SQ fit (Schroeder et al., 2005) reveals equal power with respect to temporal resolution beyond the filter frequency and required length of the time series (Fig. 3A, D). It does better with respect to the required minimum open probability (Fig. 3C). An outstanding benefit of the 2D fit is the much higher tolerance to noise (Fig. 3B) compared to the other algorithms.

Another important capability of the 2D fit is the discrimination of Markov models (Fig. 5). In theory, the direct fit of the time series (HMM) should be able to give the same results, but it turned out to be less efficient when applied to data. This comparison, however, is not quite fair because the "theoretical" data of the 2D approach are obtained from simulations which provide a perfect inclusion of noise and filtering.

The benefit of employing simulations for the "theoretical" curve (as introduced by Magleby & Weiss, 1990a) is probably also the reason for the good performance of the subsequent HMM fit (Schroeder et al., 2005). Furthermore, this became obvious in the investigations of Farokhi et al. (2000). Time series were analyzed by means of an HMM fit. However, the rate constants resulting from fitting the measured data were not taken as "true" rate constants, but sets of higher rate constants were used to simulate time series which were fitted in the same way as the measured data. Those sets which resulted in the same fitted rate constants as obtained from the measured time series were regarded as "true" rate constants. However, an automatic algorithm for the incorporation of simulations into the HMM fit remains to be developed.

Also, the improvements in the present study, i.e., usage of the LS criterion instead of ML, averaging over 9 or 25 bins (if temporal resolutions allowed it), were important ingredients of the efficiency of 2D fit. Nevertheless, Figure 2A implies that close to the correct value the fit may be guided more efficiently by the ML than the LS criterion. We have not tested whether changing the search criterion at the end of the fitting procedure would enhance parameter accuracy. Employing a Hinkley detector (Schultze & Draber, 1993) instead of a half-threshold jump detector (Magleby & Weiss, 1990a) may also have increased the efficiency of the analysis presented here. However, this was not systematically investigated.

Normalizing to time rather to transitions prevents possible runaway behavior, as revealed in preliminary studies: if the rate constants of the slow transitions are too fast, then there are not enough sojourns in the slow states and the occupation probability of the fast states increases, causing much more transitions. The resulting increase in N would lower the error sum if equations 5 and 6 were normalized to N. This can overcompensate the increase of the error sum by wrong predictions. The slow rate constants run away; i.e., they become faster and faster with increasing number of iterations of the fit routine.

A very important feature which has increased the power of 2D dwell-time analysis is a more efficient algorithm for searching the parameter space. Without the genetic algorithm implemented here, it is not possible to fit complex Markov models as they occur in real data. The necessary computing power was not available in the 1990s. Nowadays, this kind of analysis has become possible, but still the time required for a 2D dwell-time fit is approximately 100 times higher than the computing time for direct fit of the time series (HMM fit). Analyzing a time series with 10^9 data points can take up to 2 weeks on a 3-GHz personal computer. This problem will be overcome in the future with increasing computer speed. Especially, the genetic fit algorithm used by the 2D fit is well suited for the usage of parallel computing. However, one feature has to be mentioned. In multichannel analysis, required computer time increases only by $\sim$10% per additional channel, whereas the direct fit

employs m^N equations with m^N products, with m being the number of states per channel and N being the number of channels. In many cases, this renders impossible the analysis of more than two channels.

A very useful fringe benefit of the above investigations is the finding that the 2D fit can be used as a detector of the ''true'' current level (Fig. 6) when the apparent single-channel current is reduced by averaging over fast gating channel in the inevitable filter of the recording apparatus (Hansen et al., 1997; Schroeder & Hansen, 2006).

We thank Dr. Amke Caliebe for statistical advice. This work was supported by the Deutsche Forschungsgemeinschaft (Ha712/11-3, Ha 712/14-2) and the Bundesministerium für Bïldung und Forschung (03F0261A).

References

Albertsen, A., Hansen, U.P. 1994. Estimation of kinetic rate constants from multi-channel recordings by a direct fit of the time series. *Biophys. J.* **67:**1393–1403

Ashcroft, F.M. 2000. Ion Channels and Disease. Academic Press, San Diego

Ball, F.G., Rice, J.A. 1992. Stochastic models for ion channels: Introduction and bibliography. *Math. Biosci.* **112:**189–206

Ball, F.G., Sansom, M.S. 1989. Ion-channel gating mechanisms: Model identification and parameter estimation from single channel recordings. *Proc. R. Soc. Lond. B. Biol. Sci.* **236:**385–416

Ball, F.G., Yeo, G.F., Milne, R.K., Edeson, R.O., Madsen, B.W., Sansom, M.S. 1993. Single ion channel models incorporating aggregation and time interval omission. *Biophys. J.* **64:**357–374

Blunck, R., Kirst, U., Riessner, T., Hansen, U. 1998. How powerful is the dwell-time analysis of multichannel records? *J. Membr. Biol.* **165:**19–35

Caceci, M.S., Cacheris, W.P. 1984. Fitting curves to data - The simplex algorithm is the answer. *BYTE* **5/84:**340–362

Caliebe, A., Rösler, U., Hansen, U.P. 2002. A chi^2 test for model determination and sublevel detection in ion channel analysis. *J. Membr. Biol.* **185:**25–41

Charbonneau, P. 2002. An Introduction to Genetic Algorithms for Numerical Optimization. High Altitude Observatory, Boulder, CO

Colquhoun, D., Hawkes, A.G. 1977. Relaxation and fluctuations of membrane currents that flow through drug-operated channels. *Proc. R. Soc. Lond. B. Biol. Sci.* **199:**231–262

Colquhoun, D., Hawkes, A.G. 1990. Stochastic properties of ion channel openings and bursts in a membrane patch that contains two channels: Evidence concerning the number of channels present when a record containing only single openings is observed. *Proc. R. Soc. Lond. B. Biol. Sci.* **240:**453–477

Crouzy, S.C., Sigworth, F.J. 1990. Yet another approach to the dwell-time omission problem of single-channel analysis. *Biophys. J.* **58:**731–743

Doyle, D.A., Morais Cabral, J., Pfuetzner, R.A., Kuo, A., Gulbis, J.M., Cohen, S.L., Chait, B.T., MacKinnon, R. 1998. The structure of the potassium channel: Molecular basis of K^+ conduction and selectivity. *Science* **280:**69–77

Draber, S., Schultze, R. 1994. Correction for missed events based on a realistic model of a detector. *Biophys. J.* **66:**191–201

Farokhi, A., Keunecke, M., Hansen, U.P. 2000. The anomalous mole fraction effect in *Chara*: Gating at the edge of temporal resolution. *Biophys. J.* **79:**3072–3082

FitzHugh, R. 1983. Statistical properties of the asymmetric random telegraph signal with application to single channel analysis. *Math. Biosci* **64:**75–89

Fredkin, D.R., Rice, J.A. 1992. Maximum likelihood estimation and identification directly from single-channel recordings. *Proc. R. Soc. Lond. B. Biol. Sci.* **249:**125–132

Fredkin, D.R., Rice, J.A. 2001. Fast evaluation of the likelihood of an HMM: Ion channel currents with filtering and colored noise. *IEEE Trans. Sig. Proc.* **49:**625–633

Ganesan, R., Sherman, A.T. 1994. Statistical techniques for language recognition: An empirical study using real and simulated English. *Cryptologia* **18:**289–332

Hansen, U.P., Cakan, O., Abshagen-Keunecke, M., Farokhi, A. 2003. Gating models of the anomalous mole-fraction effect of single-channel current in *Chara*. *J. Membr. Biol.* **192:**45–63

Hansen, U.P., Keunecke, M., Blunck, R. 1997. Gating and permeation models of plant channels. *J. Exp. Bot.* **48:**365–382

Hawkes, A.G., Jalali, A., Colquhoun, D. 1992. Asymptotic distributions of apparent open times and shut times in a single channel record allowing for the omission of brief events. *Phil. Trans. R. Soc. Lond. B. Biol. Sci.* **337:**383–404

Hille, B. 2001. Ion Channels of Excitable Membranes. Sinauer Associates, Sunderland, MA

Holland, J. 1975. Adaptation in Natural and Artificial Systems. University of Michigan Press, Ann Arbor

Jiang, Y., Lee, A., Chen, J., Cadene, M., Chait, B.T., MacKinnon, R. 2002. Crystal structure and mechanism of a calcium-gated potassium channel. *Nature* **417:**515–522

Kienker, P. 1989. Equivalence of aggregated Markov models of ion-channel gating. *Proc. R. Soc. Lond. B. Biol. Sci* **236:**269–309

Klein, S., Timmer, J., Honerkamp, J. 1997. Analysis of multichannel patch clamp recordings by hidden Markov models. *Biometrics* **53:**870–884

Klieber, H.G., Gradmann, D. 1993. Enzyme kinetics of the prime K^+ channel in the tonoplast of *Chara*: Selectivity and inhibition. *J. Membr. Biol.* **132:**253–265

Korn, S.J., Horn, R. 1988. Statistical discrimination of fractal and Markov models of single-channel gating. *Biophys. J.* **54:**871–877

Loeptin, U. 1999. Modellidentifikation bei der Untersuchung von Ionenkanälen. Diploma thesis, University of Kiel

Long, S.B., Campbell, E.B., MacKinnon, R. 2005a. Crystal structure of a mammalian voltage-dependent *Shaker* family K^+ channel. *Science* **309:**897–903

Long, S.B., Campbell, E.B., MacKinnon, R. 2005b. Voltage sensor of Kv1.2: Structural basis of electromechanical coupling. *Science* **309:**903–908

Magleby, K.L., Weiss, D.S. 1990a. Estimating kinetic parameters for single channels with simulation. A general method that resolves the missed event problem and accounts for noise. *Biophys. J.* **58:**1411–1426

Magleby, K.L., Weiss, D.S. 1990b. Identifying kinetic gating mechanisms for ion channels by using two-dimensional distributions of simulated dwell times. *Proc. R. Soc. Lond. B. Biol. Sci.* **241:**220–228

McManus, O.B., Blatz, A.L., Magleby, K.L. 1987. Sampling, log binning, fitting, and plotting durations of open and shut intervals from single channels and the effects of noise. *Pfluegers Arch.* **410:**530–553

Michalek, S., Lerche, H., Wagner, M., Mitrovic, N., Schiebe, M., Lehmann-Horn, F., Timmer, J. 1999. On identification of Na^+ channel gating schemes using moving-average filtered hidden Markov models. *Eur. Biophys. J.* **28:**605–609

Parzefall, F., Wilhelm, R., Heckmann, M., Dudel, J. 1998. Single channel currents at six microsecond resolution elicited by acetylcholine in mouse myoballs. *J. Physiol.* **512:**181–188

Press, W.H., Flannery, B.P., Teukolsky, S.A., Vetteling, W.T. 1989. Numerical Recipes in Pascal. Cambridge University Press, Cambridge, 326–330

Qin, F., Auerbach, A., Sachs, F. 2000. Hidden Markov modeling for single channel kinetics with filtering and correlated noise. *Biophys. J.* **79:**1928–1944

Rechenberg, I. 1973. Evolutionsstrategie. Fromman-Hozboog Verlag, Stuttgart

Riessner, T. 1998. Level detection and extended beta distributions for the analysis of fast rate constants of Markov processes in sampled data. PhD diss., University of Kiel

Riessner, T., Woelk, F., Abshagen-Keunecke, M., Caliebe, A., Hansen, U.P. 2002. A new level detector for ion channel analysis. *J. Membr. Biol.* **189:**105–118

Rosales, R.A., Fitzgerald, W.J., Hladky, S.B. 2002. Kernel estimates for one- and two-dimensional ion channel dwell-time densities. *Biophys. J.* **82:**29–35

Sakmann, B., Neher, E. 1995. Single-Channel Recordings. Plenum Press, New York

Schroeder, I., Hansen, U.P. 2006. Strengths and limits of beta distributions as a means of reconstructing the true single-channel current in patch clamp time series with fast gating. *J. Membr. Biol.* **210:**199–212

Schroeder, I., Harlfinger, P., Huth, T., Hansen, U.P. 2005. A subsequent fit of time series and amplitude histogram of patch-clamp records reveals rate constants up to 1 per microsecond. *J. Membr. Biol.* **203:**83–99

Schroeder, I., Huth, T., Suitchmezian, V., Jarosik, J., Schnell, S., Hansen, U.P. 2004. Distributions-per-level: A means of testing level detectors and models of patch-clamp data. *J. Membr. Biol.* **197:**49–58

Schultze, R., Draber, S. 1993. A nonlinear filter algorithm for the detection of jumps in patch-clamp data. *J. Membr. Biol.* **132:**41–52

Schulz-DuBois, E.O., Rehberg, I. 1981. Structure function in lieu of correlation function. *Appl. Phys.* **24:**323–329

Singh, A.C., Sutradhar, B.C. 1989. Testing proportions for Markov dependent Bernoulli trials. *Biometrika* **76:**809–813

Townsend, C., Horn, R. 1999. Interaction between the pore and a fast gate of the cardiac sodium channel. *J. Gen. Physiol.* **113:**321–332

Venkataramanan, L., Kuc, R., Sigworth, F.J. 1998a. Identification of Hidden Markov models for ion channel currents - Part I: Colored background noise. *IEEE Trans. Sig. Proc.* **46:**1901–1915

Venkataramanan, L., Kuc, R., Sigworth, F.J. 1998b. Identification of Hidden Markov models for ion channel currents - Part II: State-dependent excess noise. *IEEE Trans. Sig. Proc.* **46:**1916–1929

Venkataramanan, L., Kuc, R., Sigworth, F.J. 2000. Identification of Hidden Markov models for ion channel currents - Part III: Bandlimited, sampled data. *IEEE Trans. Sig. Proc.* **48:**376–385

Venkataramanan, L., Sigworth, F.J. 2002. Applying Hidden Markov models to the analysis of single ion channel activity. *Biophys. J.* **82:**1930–1942

Wall, M.B. 1996. A genetic algorithm for resource-constrained scheduling. PhD diss., Massachusetts Institute of Technology

White, P.J., Ridout, M.S. 1998. The estimation of rapid rate constants from current-amplitude frequency distributions of single-channel recordings. *J. Membr. Biol.* **161:**115–129

Yellen, G. 1984. Ionic permeation and blockade in Ca^{2+}-activated K^+ channels of bovine chromaffin cells. *J. Gen. Physiol* **84:**157–186

Yeo, G.F., Milne, R.K., Edeson, R.O., Madsen, B.W. 1988. Statistical inference from single channel records: Two-state Markov model with limited time resolution. *Proc. R. Soc. Lond. B. Biol. Sci.* **235:**63–94

Zheng, J., Venkataramanan, L., Sigworth, F.J. 2001. Hidden Markov model analysis of intermediate gating steps associated with the pore gate of *Shaker* potassium channels. *J. Gen. Physiol.* **118:**547–564